Journal of Engineering Science and Technology
Special Issue on SU18, February (2019) 286 - 299
© School of Engineering, Taylor's University

SUSTAINABLE HIGH TORQUE FOR ELECTRIC SCOOTER PROPULSION USING PERMANENT MAGNET FLUX SWITCHING MACHINE TECHNOLOGY

MBADIWE IGNATIUS ENWELUM*,
ERWAN SULAIMAN, LIEW CHUNG PENG*

Research Centre for Applied Electromagnetics,
Universiti Tun Hussein Onn Malaysia
86400, Parit Raja, Batu Pahat, Johor Malaysia
Eclimo SDN BHD, Jalan Lima Tanjung Tokong, 10470 Penang Malaysia
*Corresponding Author: Mb.fkee.uthm@gmail.com

Abstract

The use of permanent magnet electric motor in electric scooter and vehicles for propulsion device has successively eliminated combustion engine in them. Presently, Permanent Magnet Synchronous Motor (PMSM), Type Radial Hub has been developed and installed for propulsion in Electric Scooter, Model ES11. The motor is three-phase consisting of 4-segmented stator cells and 20 rotor pole, which employed all stator teeth winding, utilizing 2 kg permanent magnet weight. The output torque and power of motor are 110 Nm and 6 kW. Unfortunately, this performance could not sustain acceleration for long driving range due to mounted permanent magnets on the rotating rotor, which get heated at high temperature. Furthermore, PMSM lacks proper mechanical assembly and strength for speed operation. To overcome these challenges, this paper presents a different type of synchronous motor, flux switching motor using permanent magnet excitation and employing isolated rotor segments bonded by an external envelope. The motor, a three-phase winding consists of 24/14 stator-segment rotor and utilizing 1 kg mass of permanent magnet in a radial direction and armature winding in an alternate pattern. The JMAG Tool Solver, version 14 was used for the simulation and the two-dimensional Finite Element Analysis (2D-FEA) in terms of magnetic flux, cogging torque, flux strengthening and torque respectively. Results of performance showed proposed motor achieved average torque of 241 Nm representing 2.19 times higher and constant output power of 35 kW presenting 5.8 times higher than the conventional motor, thereby projecting proposed motor as a better motor type for higher torque suitable for scooter propulsion than PMSM.

Keywords: Flux switching motor, High torque, In-wheel application, Isolated rotor segments, Permanent magnet.

1. Introduction

It is already over a century that combustion engine vehicles have dominated the transportation sector [1-3]. Unfortunately, the use of fossil fuel in combustion engine has contributed to the increasing emission of carbon dioxide to the environment, which poses major concerns to everyone. As a practical measure by the government and relevant sectors to control this emission menace, vehicles propelled by electric motors and powered by electricity stored in the battery are the viable solution [4-6]. Currently, considerable developments have been achieved in electric vehicles, which use electric motors for propulsion [7-10]. As torque is the principal factor and rotational force that overcomes inertia and sustains acceleration, the design of high torque motor is necessary for effective performance. At present, conventional electric scooters and electric vehicles are being propelled by electric motors having low torque capability that would not sustain acceleration for long distance travel [2]. For this reason, electric motors for high vehicles propulsion are traditionally structured to meet basic requirements such as fast torque response, rated constant power and high torque on driving conditions of acceleration [11, 12].

Four electric motors have been investigated and developed for high torque namely; permanent magnet direct current (PMDC) motor, switched reluctance motor (SRM), permanent magnet synchronous motor (PMSM) and induction motor (IM) [13-16]. Meanwhile, the characteristics performance of PMDC had fallen short of long driving operation because it demands regular maintenance with regular replacement of carbon brush [17-20]. On the part of SRM, though it has a simple construction and low manufacturing cost, rugged and used in every hostile environment, fault-tolerant capability and simple control, it exhibits high torque ripple and a significant acoustic noise [21, 22]. On the part of IM with squirrel cage rotor is a good contender due to its ruggedness, reliability, low-cost, low maintenance and capable of operating in a harsh environment, its downsides include low efficiency, low power density and low power factor, which are not necessary for propulsion drives [22]. These problems have made IM to be ignored for use.

Furthermore, PMSM especially, the rotor mounted permanent magnet synchronous motor (RPMSM) was developed to meet the requirements of high torque, however, a close relationship does not exist between the torque, speed curve and motor parameters [13]. It consists of a segmented stator with all tooth armature winding and mounted permanent magnets rotating the round rotor. While the motor generated promising average output torque of 110 Nm and power of 6 kW, it lacks the mechanical assembly to operate at the high-temperature condition. Figure 1 shows the cross-sections of the conventional three-phase segmented stator PMSM.

To overcome the downsides associated with the RPMSM, a reliable motor must have constant high torque and power such as flux-switching machine (FSM). FSM is an advanced form of a synchronous motor having the structure of inductor generator and switched reluctance motor, making it mechanically fit for driving operation [14]. FSM has numerous advantages as compared to previous generations of AC motors [23-26]. FSM type of AC motor locates all active parts in the stationary stator leaving rotor without carrying any material [27, 28]. There are three internal kinds of FSM due to each peculiar flux source such as; a permanent magnet (PM) FSM, field excitation (FE) FSM and hybrid excitation (HE) FSM

[29]. PM, FE and HE (combines both PM and FE) as main and secondary flux sources. Of the types of FSM, the PMFSM offers loss-free excitation and providing higher torque density than others. More advantages of PM motors include rugged structure, high efficiency and good flux weakening capability [14, 30].

While numerous designs have been in the inner rotor for out-wheel application, research and development have not focused on outer rotor configuration suitable for in-wheel application such as electric motor-bike that eliminates combustion engine [15]. In the same vein, salient rotor pole motors have dominated motor design and development for so long while less attention has been given to explore the gains associated with segmented rotor [28, 29]. For an in-wheel application, a conventional inner rotor is transferred to outer structure [30]. Outer rotor PMFSMs in salient rotor have been widely designed and discussed [21] in which, the electromagnetic issues have been addressed. These design recorded low rated torque suitable for light-weight application [19].

As discussed by Zulu et al. [29], the torque performance of FSM has been improved using the rotor segment. It was designed in such, as to accomplish a two-way flux linkage in the same segment and in addition, favour alternate armature stator teeth winding. This guarantees high flux linkage due to shorter end windings resulting in less conductor usage.

This paper presents a three-phase Permanent Magnet Flux-Switching Motor (PMFSM) with respect to rotor transition and structure configuration. PMFSM in rotor segments transferred from inner to the outer position will rotate slowly and generate higher torque than the salient rotor. In the preceding sections, the motor's output equation is established and high magnetic loading is required, confirmation of feasible stator-rotor combination for four set of armature alternate stator tooth winding, motor design and modeling, results and performance analysis in terms of peak magnetic flux, cogging torque, counter-electromotive force, flux strengthening and average torque.

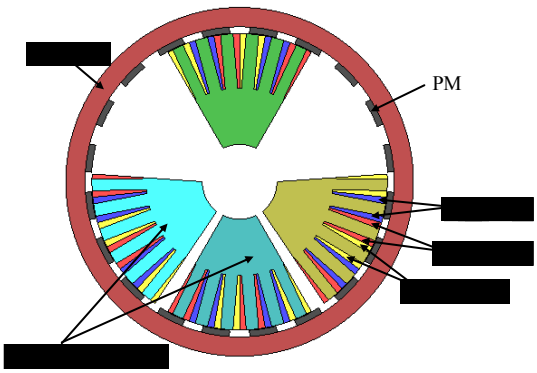

Fig. 1. Three-phase segmented stator PMSM.

2. Output Equation of Motor

Output equation of the electric motor is given as a two set of loading parameters such as; magnetic loading and electrical loading in (1).

$$Q = C_O D^2 L \mathrm{N_S} \tag{1}$$

where Q = Power in watts, $C_o = \pi^2 B_{av} a.c$

C_o is the output coefficient of the conductor, D is the diameter of the motor, L is stack length, N_s is the speed of the motor in rev/min.

Meanwhile, components of the output equation, the magnetic and electric loading of the machine is as in Eqs. (2) and (3).

$$B_{av} = \frac{p\Phi}{\pi DL} \tag{2}$$

where B_{av} is average flux density, p is the number of poles, Φ is magnetic flux.

$$a.c = \frac{NI}{\pi D} \tag{3}$$

Where N is the number of conductors, I is input current.

Substituting Eqs. (2) and (3) into Eq. (1):

$$Q = (\pi^2) * (\frac{p\Phi}{\pi DL}) * (\frac{NI}{\pi D}) * (D^2 L) * (N_s) \tag{4}$$

Magnetic loading $\frac{p\Phi}{\pi DL}$, electrical loading $\frac{NI}{\pi D}$, the mechanical part $D^2 L$ and speed of the motor N_s. When the electric supply and other restrictions are kept constant, the proposed motor torque equation depends on specific magnetic loading, flux per pole (Φ/p). Hence, rotor pole design is the determinant factor. For the proposed motor, design restrictions and specifications are the same with PMSM shown in Fig. 1.

3. Research Method

The commercial JMAG Designer Tool Solver version 14, is used in the design and 2-D FEA simulation analysis. Material for both rotor and stator core is electromagnetic steel 35H210, PM is Neomax-35AH. Parameter specifications, restriction and electric supply related to inverter are listed in Table 1. The peak armature current density is set at 30 A/mm^2, the diameter of the motor is 279.4 mm and a stack length of 100 mm, the same with conventional RPMSM.

The target torque of the proposed motor is set to be higher than 110 Nm with constant output power load. For the isolated segments to be mechanically secured, an external envelop made of aluminium is employed without adding excessive weight. For the initial rotor angle, design geometry followed the convention given in Eq. (5).

$$Rotor\ \ angle\ \ \theta = \frac{360\ ^\circ x\ R_W}{2\pi\ x\ R_{ir}} \tag{5}$$

Segment span angle $\theta_S = \theta + x$.

where R_w is the rotor width, R_{ir} inner rotor radius, $1° \leq x \leq 3°$.

Table 1. Design specification, parameter restrictions and electric supply.

Parameter description	Segmented stator PMSM	Segmented rotor PMFSM
Diameter of motor (mm)	297.4	297.4
No. of phase	3	3
Type of rotor	Cylindrical/round	Segmented
No. of rotor pole	100	14
Type of pole	Toothed	Segmented
No. of stator pole	18	12
Type of stator	Segmented	Toothed
Air- gap length (mm)	0.5	0.5
Stack- length	100	100
DC voltage inverter (V)	415	415
Inverter current (A_{rms})	360	360
Armature slot area (mm^2)	NA	432
Location of active parts	Stator/rotor	Stator
No. of conductor	18	18
Average torque (Nm)	110	>>>110
Power output (kW)	6	>>6
Speed of motor (rev/min.)	1900	<1900

3.1. Rotor segment design

According to Galea et al. [13], Fig. 2 illustrates the rotor segment shapes considered. The rotor segment shape, transverse in Fig. 2(a) shows the geometry employed with compromise, however, it lacks provision for any form of direct fixing.

Figure 2(b) is a dove-tail segment designed for unbalanced fixation. As shown in Fig. 2(c) it is a groove type, however, is a lower torque output. Therefore, knowing these limitations, transverse rotor segment has been modified with respect to length and angle to ensure maximum flux flow as shown in Fig. 2(d).

Therefore, Fig. 3 presents the cross-sections of a designed three-phase PMFSM in the segmented outer rotor.

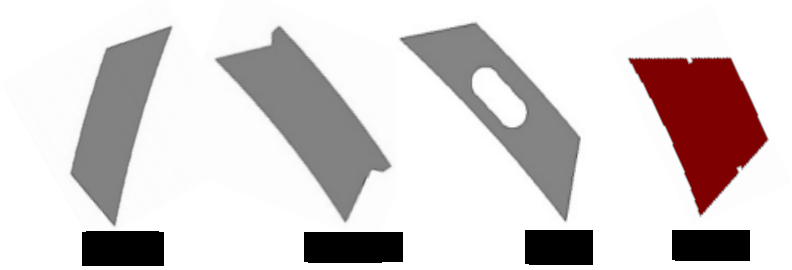

Fig. 2. Rotor segments under consideration: (a)Transverse segment, (b) Dovetail segment, (c) Groove segment, (d) Modified transverse segment.

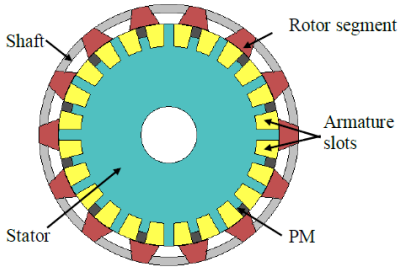

Fig. 3. Cross-section of three-phase segmented outer rotor 12S/14P PMFSM.

3.2. Operating principle

In order to understand the principle of operation of segmented rotor PMFSM in out-runner, the rectilinear cell arrangement is presented in Fig. 4. The flux-switching mechanism is explained using (permanent magnet) PM1 and armature coil. At the initial condition when stator tooth is in alignment with rotor S1, there is flux flow from PM1 into S1 in the upward direction linking with S1 and back to the stator back-iron as shown in Fig. 4(a). However, in the second alignment, when segment rotor S1 begins to rotate in a counter-clockwise direction, flux begins to flow from PM2 through S1 into the stator pole. Therefore, as S1 continues to rotate and at the third quadrant, there is a switch of flux at the same stator teeth from PM2 to the downward direction as shown in Fig. 4(b).

The operating principle of the proposed segmented outer rotor PMFSM was examined and confirmed before proceeding for the motor analysis. As it concerns flux switching, the U-phase from the flux supposedly has a maximum amplitude at 90 degrees of the electrical cycle to contribute to flux linkage interaction between the flux armature and the PM. Confirming the operating principle flows the procedure for coil test. Coil test of PMFSM is conducted with the four set of coils in an identical manner of sinusoidal waveform separated by 120° apart. The results obtained from the characteristics of fluxes produced a three different groups of fluxes. The flux linkage at each coil phase is observed and the armature coil phases are identical to the conventional balance of the three-phase U, V and W, as depicted in Fig. 5.

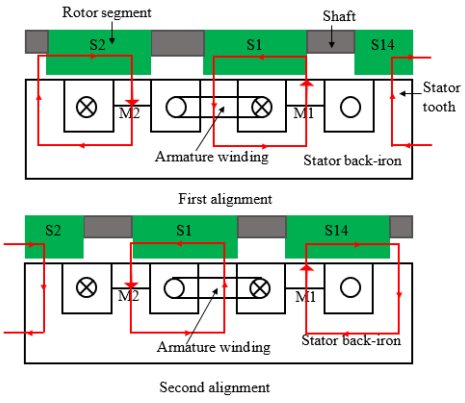

Fig. 4. Operating principle of segmented outer rotor PMFSM: (a) First alignment, (b) Second alignment.

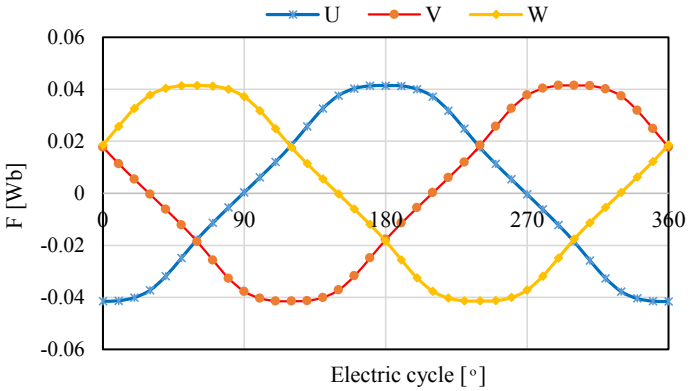

Fig. 5. Three-phase magnetic flux linkage of proposed motor.

3.3. Motor model

In Fig. 5, the three-phase flux linkage due to PM in the proposed 24S/14P PMFSM is illustrated. According to the FSM mechanism, flux linkage changes with rotor position θ_r. Meanwhile, in PMFSM, flux is produced by PM on no-load located in the stator and furthermore, when current is applied to the phase winding on the stator. Jia et al. [31] expressed that for the sake of this modelling, flux is due when current is applied to phase winding is neglected, thus, the PM flux linkage ψ_m, corresponding to 3φ windings.

$$\psi_m 3\varphi = \begin{bmatrix} \psi_{mU} = \psi_m cos(P\theta_r) \\ \psi_{mV} = \psi_m cos(P\theta_r - \frac{2\pi}{3}) \\ \psi_m W = \psi_m cos(P\theta_r + \frac{2\pi}{3}) \end{bmatrix} \tag{6}$$

where ψ_m is the magnitude of the flux linkage, P is the number of rotor pole and θ_r is rotor position.

In the same vein, armature inductances for 24S/14P PMFSM, based on finite element analysis, the path of flux at any position through the air-gap around will pass two rotor poles. Therefore, self-inductances for the three-phase are given as:

$$L3\varphi = \begin{bmatrix} L_{UU} = L_o - L_m cos(2P\theta_r \\ L_{VV} = L_o - L_m cos(2P\theta_r + \frac{2\pi}{3}) \\ L_{WW} = L_o - L_m cos(2P\theta_r - \frac{2\pi}{3}) \end{bmatrix} \tag{7}$$

where L_o is self- inductance and L_m is the magnitude of the fundamental part. Meanwhile, mutual-inductances are expressed as:

$$M3\phi = \begin{bmatrix} M_{UV} = M_{VU} = M_o - M_m cos(2P\theta_r - \frac{2\pi}{3}) \\ M_{VW} = M_{WV} = M_o - M_m cos(2P\theta_r) \\ M_{WU} = M_{UW} = M_o - M_m cos(2P\theta_r + \frac{2\pi}{3}) \end{bmatrix} \quad (8)$$

where M_o is the mutual inductance and M_m is the magnitude of the fundamental part.

Furthermore, the direct axis to the quadrature axis of transformation from the stator reference frame to the rotor frame, are clearly defined in Fig. 6. Rotor position B1 is chosen where the flux linkage of PM is maximum, the quadrature axis is lagging the direct axis as depicted in Fig. 6. The stator to flux association based on the synchronous reference frame using Park's transformation matrix is given as:

$$P = \frac{2}{3}\begin{bmatrix} cos\,\theta_a & cos\,(\theta_a - \frac{2\pi}{3}) & cos\,(\theta_a + \frac{2\pi}{3}) \\ -sin\theta_a & -sin\,(\theta_a - \frac{2\pi}{3}) & -sin\,(\theta_a + \frac{2\pi}{3}) \\ \frac{1}{2} & \frac{1}{2} & \frac{1}{2} \end{bmatrix} \quad (9)$$

where θ_a is rotor angle between the coil phase and the direct axis, equal to $P_r\theta_r$.

Using Eqs. (6) and (9), transforming the PM flux linkages in the rotor reference frame ψ_{md} and ψ_{mq} give:

$$\psi_{mdq} = \begin{bmatrix} \psi_{md} = \psi_m \\ \psi_{mq} = 0 \end{bmatrix} \quad (10)$$

Equation (10) shows PM flux linkages transformed in the d-axis and q-axis. Noticeably, transforming the three-phase inductance in rotor pole frame, the PMFSM can be described as given:

$$L_{dq0} = \begin{bmatrix} L_d = L_o - M_o - \frac{3}{2}\left[\frac{L_d - L_q}{3}\right] \\ L_q = L_o - M_o + \frac{3}{2}\left[\frac{L_d - L_q}{3}\right] \\ L_o = L_{dq} = L_{qd} = L_{d0} = 0 \end{bmatrix} \quad (11)$$

$$\left[L_o - M_o = \frac{1}{2}(L_d + L_q)\right]$$

where $L_d, L_q, L_0, L_{dq}, L_{qd}$ are inductance components transformed in the rotor reference frame. Therefore, the sum of d-axis and q-axis flux linkages expression confirm the equation stated.

$$\begin{bmatrix} \psi_d = L_d i_d = \psi_m + \{L_o - M_o - \frac{3}{2}(\frac{L_d - L_q}{3})\} i_d \\ \psi_q = L_q i_q = \{L_o - M_o - \frac{3}{2}(\frac{L_d - L_q}{3})\} i_q \end{bmatrix} \tag{12}$$

Moreover, the voltage equations in the d-axis and q-axis are obtained and expressed as:

$$u_{dq} = \begin{bmatrix} u_d = R_c i_d + \frac{\partial \psi_d}{\partial t} - \omega_c \psi_q \\ u_q = R_c i_q + \frac{\partial \psi_q}{\partial t} + \omega_c \psi_d \end{bmatrix} \tag{13}$$

where R_c is the reactance of the winding coil, ω_c the frequency of the inverter

Therefore, the electromagnetic torque, T_{em} of PMFSM is given in Eq. (14):

$$T_{em} = \frac{3}{2} P_r \left[\psi_m i_q + (L_d - L_q) i_d i_q\right] \tag{14}$$

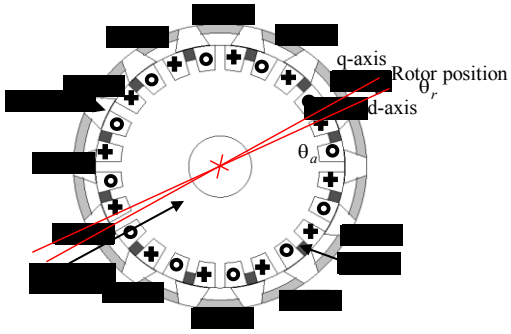

Fig. 6. Consideration of direct axis - quadrature axis definitions of PMFSM.

4. Performance Analysis

The performances of the motor in open and closed circuit conditions: Under open circuit condition include; cogging torque analysis and harmonics order. Close circuit condition includes; flux strengthening, torque versus armature current density, torque versus speed characteristics, average torque and power are discussed under the following subsections.

4.1. Cogging torque and harmonic order

Cogging torque of the proposed motor at a rotation of 1900 rev/min on open circuit, is shown in Fig. 7. While cogging torque does not contribute to an output torque of the motor, it should be as minimal as possible to ensure that the motor operates safely. Meanwhile, cogging torque is the factor that causes noise and

vibration when it is high [32]. In Fig. 7, the cogging torque value is 16Nm peak-to-peak with waveform characterized by space harmonics. Based on studies by Liang and Luy [32], this harmonic is produced by magnetic interacting with various phase windings to create the rotating field. However, space harmonics can be reduced and not completely eradicated. Hence, Fig. 8 depicts the magnitudes of harmonic order with the lowest amplitude at 11th order.

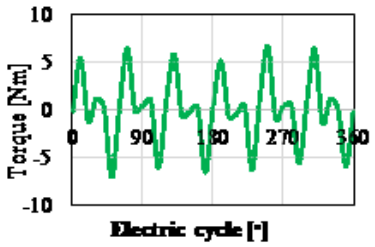

Fig. 7. Cogging torque of PMFSM.

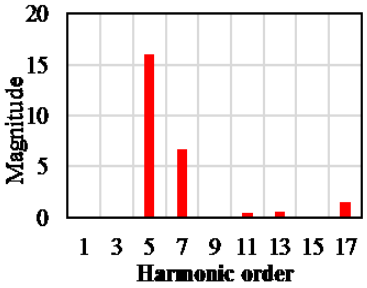

Fig. 8. Magnitudes of order with rotor.

4.2. Flux strengthening of proposed PMFSM

Flux strengthening of the proposed machine was observed with PM only and furthermore of armature current density. At initial condition when the rotor is aligned with stator pole, flux due to PM only is maximum.

Shown in Fig. 9 is the U-phase magnetic flux of PM and maximum cutting the x-axis at 90 ° and 270 °.

However, by injecting current density of different values, the rotation of rotor now aligns with another stator pole, flux value increases linearly and sharply with lower current values of J_a 5 A/mm^2 and J_a 10 A/mm^2 and lagging behind each other at the peak value of PM cutting the x-axis at 0 ° and 180 °. Figure 10 depicts the flux strengthening plot of the proposed PMFSM design.

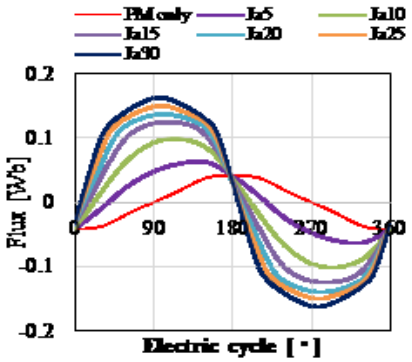

Fig. 9. Magnetic flux of PMFSM.

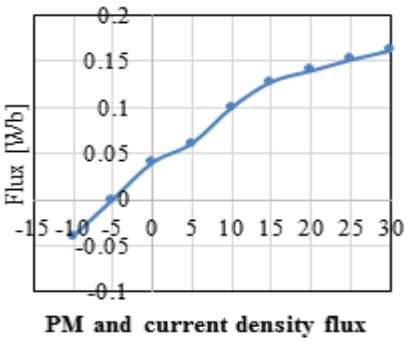

Fig. 10. Max. flux linkage of PMFSM.

4.3. Torque against current density and torque against speed of PMFSM

The characteristics of torque of the proposed PMFSM in the segmented rotor is examined at armature current density varied from J_a 5 A/mm^2 to the peak value of J_a 30 A/mm^2 respectively.

It is seen in the plot shown in Fig. 11 that output torque increases, however, not directly proportional with an increase in current density. At lower current value, there is linearity, however, not directly proportional with an increase in armature current value.

Meanwhile, the torque plot against speed is shown in Fig. 12 in which, at the base speed of 1,397 rev/min, the maximum torque of 241 Nm is obtained and is constant within the torque region.

However, when the motor is operated beyond the base speed, the torque will start to decrease while operating at the higher speed resulting in a high iron loss.

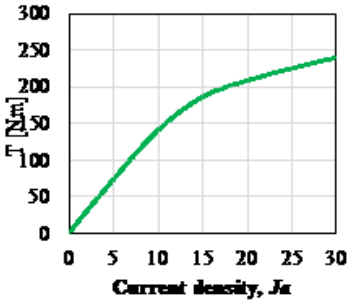

Fig. 11. Torque against current density.

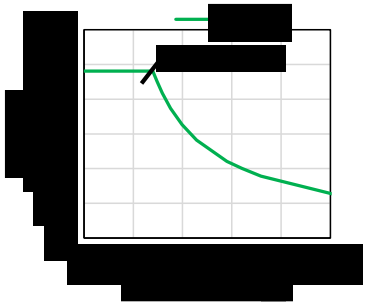

Fig. 12. Torque against speed.

4.4. Torque profile against output power of proposed PMFSM

The torque against output power performance of the proposed machine is illustrated in Fig. 13. It is seen that the maximum output torque is 241 Nm and in addition, motor-generated constant power of 35 kW. A cursory look at the plot, it is clear that output power remained constant throughout the torque load region. This characteristic proves the viability and reliability of the proposed motor to sustain acceleration.

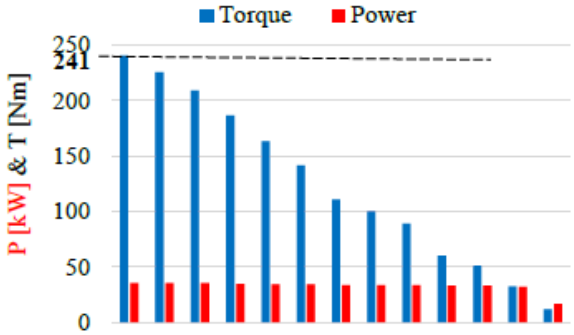

Fig. 13. Torque against output power characteristics.

5. Conclusions

In this paper, segmented outer rotor flux-switching machine using permanent flux source has been designed and presented for electric scooter (electric vehicle) application. It consists of 24/14 stator-rotor poles with alternate stator armature winding on 12 stator poles while the remaining stator poles were mounted permanent magnets in a radial direction. The segmented rotors are bound using external envelope made of aluminium for retainment for proper mechanical assembly without adding excessive material. The 2-D FEA was conducted using JMAG Tool Solver version 14. The machine is low-cost, which utilized 1 kg mass of PM representing less than which, is used in conventional RPMSM employed in Malaysian electric scooter, model ES11. The output torque of the proposed motor is 241 Nm presenting 2.1 times higher than the RPMSM. This performance projects PMFSM in a segmented rotor, as a viable and reliable candidate for high torque needed to easily overcome inertia and sustain acceleration for long distance travels.

Acknowledgement

This research work was sponsored by Research and Management Centre, Universiti Tun Hussein Onn Malaysia (UTHM) and FRGS Grant Vot 1651 under Ministry of Education, Malaysia.

References

1. Kumar, H.; and Ravikumar, S. (2010). An approach of co_2 capture technology for mitigating global warming and climate change - an overview. *Proceedings of the Conference on Recent Advances in Space Technology Services and Climate Change.* Chennai, India, 364-371.
2. Bose, B.K. (2010). Global warming: Energy, environmental pollution and the impact of power electronics. *IEEE Industrial Electronics Magazine* 4(1), 6-17.
3. Alexander, M. (2015). *Environmental assessment of full electric transportation portfolio*. Palo Alto, California: Electric Power Research Institute (EPRI).
4. Anekunu, A.Y.; Chowdhury, S.P.; and Chowdhury, S. (2013). A review of research and development on switched reluctance motor for electric vehicles. *Proceedings of the Power and Energy Society General Meeting*. Vancouver, Canada, 1-5.
5. Labak, A.; and Kar, N.C. (2012). Outer rotor switched reluctance motor design for in-wheel drive electric bus applications. *Proceedings of the 20th International Conference on Electrical Machines*. Marseille, France, 418-423.
6. Dorrell, D.G.; Popescu, M.; Evans, L.; Staton, D.A.; and Knight, A.M. (2010). Comparison of permanent magnet drive motor with a cage induction motor design for a hybrid electric vehicle. *Proceedings of the International Power Electronics Conference.* Sapporo, Japan, 1807-1813.
7. Nikam, S.P.; Rallabandi, V.; and Fernandes, B.G. (2012). A high-torque-density permanent-magnet free motor for in-wheel electric vehicle application. *IEEE Transactions on Industry Applications,* 48(6), 2287-2295.
8. Chen, X.; Deng, Z.; Peng, J.; and Li, X. (2010). Comparison of two switched reluctance motors with bipolar excitation. *Proceedings of the 5th IET*

International Conference on Power Electronics, Machines and Drives (PEMD). Brighton, United Kingdom, 1-6.

9. Xue, X.D.; Cheng, K.W.E.; Ng, T.W.; and Cheung, N.C. (2010). Multi-objective optimization design of in-wheel switched reluctance motors in electric vehicles. *IEEE Transactions on Industrial Electronics,* 57(9), 2980-2987.
10. Chiba, A.; Takano, Y.; Takeno, M.; Imakawa, T.; Hoshi, N.; and Takemoto, M. (2010). Torque density and efficiency improvements of a switched reluctance motor without rare-earth material for hybrid vehicles. *IEEE Transactions on Industry Applications*, 47(3), 1240-1246.
11. Waide, P.; and Brunner, C.U. (2011). *Energy-efficiency policy opportunities for electric motor-driven systems*. Paris, France: International Energy Agency.
12. Widmer, J.D.; and Mecrow, B.C. (2013). Optimised segmental rotor switched reluctance machines with a greater number of rotor segments than stator slots. *IEEE Transactions on Industry Applications,* (49)4, 1491-1498.
13. Galea, M.; Gerada, C.; and Hamiti, T. (2010). Design considerations of an outer rotor field wound flux switching machine. *Proceedings of the 20th International Conference on Electrical Machines* (ICEM). Marseille, France, 171-176.
14. Bianchi, N.; Bolognani, S.; and Zigliotto, M. (2001). High-performance PM synchronous motor drive for electrical scooter. *IEEE Transactions on Industry Applications*, (37)5, 1348-1355.
15. Fei, W.; Luk, P.C.-K.; Lu, S.; Shen, J.X.; Wang, Y.; and Jin, M. (2012). A novel permanent magnet flux switching machine with an outer rotor configuration for in-wheel light traction application. *IEEE Transactions on Industry Applications*, (48)5, 1496-1506.
16. Fodorean, D.; and Szabo, L. (2012). Control of a permanent magnet synchronous motor for electric scooter application. *Proceedings of the International Symposium on Power Electronics, Electrical Drives, Automation and Motion.* Sorento, Italy, 1178-1181.
17. Song, B.-M.; Chang, K.-C; and Choi, J.-Y. (2010). Design of an outer-rotor-type permanent magnet motor for electric scooter propulsion systems. *Proceedings of the International Power Electronics Conference - ECCE ASIA*. Sapporo, Japan, 2763-2742.
18. Sulaiman, E.; and Kosaka, T. (2012). Parameter sensitivity study for optimization of field-excitation flux switching synchronous machine for hybrid electric vehicles. *Proceedings of the 7th IEEE Conference on Industrial Electronics and Applications* (ICIEA). Singapore, 52-57.
19. Jenal, M; Sulaiman, E.; Omar, M.F.; Romalan, G.M.; and Somooro, H.A. (2015). Development of a novel permanent magnet flux switching machine prototype for light weight electric vehicle. *Proceedings of the IEEE Student Conference on Research and Development* (SCOReD). Kuala Lumpur, Malaysia, 739-744.
20. Hua, W.; Su, P.; Zhang, G.; and Cheng, M. (2015). A novel rotor-permanent magnet flux- switching machine. *Proceedings of the 10th International Conference on Ecological Vehicles and Renewable Energies* (EVER). Monte Carlo, Monaco, 1-10.

21. Fei, W.; Luk, P.C.-K., P.C.L.; Xia, B.; and Wu, D. (2013). Design improvement of outer rotor permanent magnet flux switching machine for direct drive urban electric vehicle propulsion. *Proceedings of the 39th Annual Conference on the IEEE Industrial Electronics Society*. Vienna, Austria, 7319-7324.
22. Ifedi, C.J.; Mecrow, B.C.; Broakway, S.T.M.; Boast, G.S; Atkinson, G.J.; and Kostic-Perovic, D. (2011). Fault tolerant in-wheel motor topologies for high performance electric vehicles. *IEEE Transactions on Industry Applications*, 49(3), 1249-1257.
23. Fei, W.; Luk, P.C.-K.; Shen, J.X.; Wang, Y.; and Jin, M. (2012). A novel permanent magnet flux switching machine with an outer rotor configuration for in-wheel light traction applications. *IEEE Transactions on Industry Applications*, 48(5), 1496-1506
24. Jenal, M.; and Sulaiman, E. (2015). Investigative study of a novel permanent magnet flux switching machine employing alternate circumferential and radial permanent magnet. *ARPN Journal of Engineering and Applied Sciences*, 10(15), 6513-6519.
25. Husain, I. (2005). *Electric and hybrid vehicles: Design fundamentals* (2nd ed.) Boca Raton, Florida: CRC Press.
26. Chen, J.T.; Zhu, Z.Q.; Iwasaki, S.; and Deodhar, R. (2010). A novel E-core flux switching PM brushless AC machine. *Proceedings of the IEEE Energy Conversion Congress and Exposition*. Atlanta, Georgia, United States of America, 3811-3818.
27. Lungoci, C.M.; Georgescu, M.; and Calin, M.D. (2012). Electrical motor types for vehicle propulsion. *Proceedings of the 13th International Conference on Optimization of Electrical and Electronic Equipment* (OPTIM). Brasov, Romania, 635-640.
28. Ahmad, M.Z.; Sulaiman, E.; S.; Khan, F.; and Haron, Z.A. (2014). Electromagnetic flux analysis on a new outer rotor hybrid excitation flux switching machine. *Proceedings of the IEEE Asia-Pacific Conference on Applied Electromagnetics* (APACE). Johor Bahru, Malaysia, 175-178.
29. Zulu, A.; Mecrow, B.C.; and Armstrong, M. (2012). Permanent-magnet flux-switching synchronous motor employing a segmental rotor. *IEEE Transactions on Industry Applications*, 48(6), 2259-2267.
30. Ali, H.; Sulaiman, E.; Jenal, M.; and Omar, M.F. (2015). Three phase segmental rotor hybrid excitation flux switching motors for various applications. *Proceedings of the IEEE Students Conference on Research and Development* (SCOReD). Kuala Lumpur, Malaysia, 373-377.
31. Jia, H.; Cheng, M.; Hua, W.; Lu, W.; and Fu, X. (2008). Investigation and implementation of control strategies for flux-switching permanent magnet motor drives. *Proceedings of the IEEE Industry Applications Society Annual Meeting*. Edmonton, Canada, 1-6.
32. Liang, X.; and Luy, Y. (2006). Harmonics analysis in induction motors. *Proceedings of the Conference on Electrical and Computer Engineering*. Ottawa, Ontario, Canada, 172-177.